Tensile test microcalorimetry for thermomechanical behaviour law analysis

Germain Martin, André Chrysochoos

▶ **To cite this version:**

Germain Martin, André Chrysochoos. Tensile test microcalorimetry for thermomechanical behaviour law analysis. Materials Science and Engineering: A, 1989, 108, pp.25-32. 10.1016/0921-5093(89)90402-4 . hal-03339684

HAL Id: hal-03339684
https://hal.science/hal-03339684v1

Submitted on 9 Sep 2021

HAL is a multi-disciplinary open access archive for the deposit and dissemination of scientific research documents, whether they are published or not. The documents may come from teaching and research institutions in France or abroad, or from public or private research centers.

L'archive ouverte pluridisciplinaire **HAL**, est destinée au dépôt et à la diffusion de documents scientifiques de niveau recherche, publiés ou non, émanant des établissements d'enseignement et de recherche français ou étrangers, des laboratoires publics ou privés.

Tensile Test Microcalorimetry for Thermomechanical Behaviour Law Analysis

ANDRÉ CHRYSOCHOOS and GERMAIN MARTIN

Laboratoire de Mécanique Générale des Milieux Continus, Place E. Bataillon, 34060 Montpellier Cédex (France)

Abstract

An experimental method is described for observing the energy phenomena accompanying elastoplastic deformation, in order to take them into account when identifying a behaviour law. After the energy balance has been considered, the relationships between the dissipation, the stored energy of cold work and the hardening state variables are reviewed. The dissipation is measured continuously during monotonic tensile tests, using microcalorimetry techniques. We describe the experimental arrangement using physical hypothesis and mathematical modelling which allow us to relate the dissipated energy to the signal given by the microcalorimeter. The calibration protocol and some results on two materials are presented. In spite of the spread in experimental results, criteria can be stated for controlling the energy consistency of models.

Finally the large discrepancy between energy predictions of certain classical behaviour laws and the stored energy measurements is indicated.

1. Introduction

Deformation processes nearly always modify the temperature field of the strained material. The thermal effects accompanying the deformation have been being observed for a long time by experimentalists [1–5], but their observations concerning thermomechanical couplings are rarely taken into account in the determination of the behaviour law, even if, from a theoretical point of view, thermodynamics are omnipresent in the construction of a model [6, 7].

2. Theoretical background

For a volume V_0 of elastoplastic material, the deformation energy W_{ext} can be decomposed into an elastic (reversible) part W_e and a complementary part W_a which can also be decomposed into the dissipated energy W_d and the stored energy of cold work W_s:

$$W_{ext} = W_e + W_d + W_s. \tag{1}$$

This decomposition is described in Fig. 1 where a supplementary term W_{is} appears during loading and elastic unloading. It is called the "isentropic" energy and comes from the thermoelastic couplings; this heat supply is associated with the temperature variations of the material when transformation is reversible and adiabatic (*i.e.* isentropic). The thermomechanical process (O, A, B) represents the load–unload cycle. The complete energy balance shows that the stored

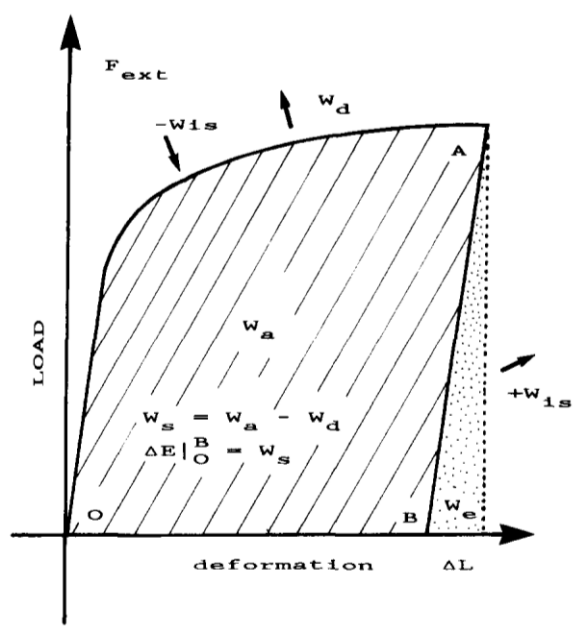

Fig. 1. Energy balance during a load–unload cycle: hatched area, anelastic work; shaded area, elastic energy; arrows, heat exchange with the surroundings.

energy variations can be considered as the internal energy variations ΔE of the material:

$$\Delta E\Big|_{O}^{A} = W_{ext} + W_{is} - W_{d} \tag{2a}$$

$$\Delta E\Big|_{A}^{B} = -W_{is} - W_{e} \tag{2b}$$

$$\Delta E\Big|_{O}^{B} = W_{s} \tag{3}$$

The use of the classical results of continuous media thermodynamics [6, 7] allows us to define the intrinsic dissipation D_1:

$$D_1 = \sigma : D - \rho \frac{\partial \psi}{\partial \alpha_j} \dot{\alpha}_j \tag{4}$$

where σ is Cauchy's stress tensor, D is the strain rate tensor and $\rho(\partial\psi/\partial\alpha_j)\alpha_j$ is the power associated with the set of the internal state variables α_j, $j = 1, 2, \ldots, n$, as a function of the Helmholtz free energy $\psi(T, \alpha_j)$ ($\alpha_0 = T$ being the absolute temperature) and ρ is the mass density. Generally, α_1 is identified as an elastic strain tensor and the set of variables α_j, $j = 2, \ldots, n$, characterizes the hardening state. Thus $\rho(\partial\psi/\partial\alpha_j)$, $j = 2, \ldots, n$, can be interpreted as residual stresses associated with the stored energy.

If we assume that the (small) temperature variations induced by deformation do not modify the hardening state ($\rho T(\partial^2\omega/\partial T\partial\alpha_j)\dot{\alpha}_j \approx 0$, $j = 2, \ldots, n$), the dissipation and the isentropic power are both mechanical heat sources present in the heat conduction equation:

$$\rho C_\alpha \dot{\theta} + \operatorname{div} \boldsymbol{q} = D_1 + \rho T \frac{\partial^2 \psi}{\partial T \partial \alpha_1} \dot{\alpha}_1 = \dot{w}_{ch} \tag{5}$$

where $\theta = T - T_a$ (T_a is the room temperature assumed to be constant) and $\boldsymbol{q}$ ($= -k \operatorname{grad} \theta$ according to Fourier's law) is the heat influx and $\dot{w}_{ch}$ is the heat source per unit volume when the external heat supply is time independent.

3. Mechanical measurements

In homogeneous tensile tests, on the assumption of a linear and isotropic law for the elastic behaviour, the load and the deformation signals give an evaluation of the axial components of the stress σ and of the elastic strain ε_e and plastic strain ε_p, which are used to calculate the anelastic energy and the isentropic energy:

$$W_a = V_0 \int_0^{\varepsilon_p(t)} \sigma \, d\varepsilon_p \tag{6}$$

$$-W_{is} \approx -\int_0^t \int_{\Omega(\tau)} \lambda T_a \operatorname{tr} \dot{\sigma} \; dx \, d\tau = -V_0 \lambda T_a \{\sigma(t) - \sigma(0)\} \tag{7}$$

λ being the linear thermal dilatation coefficient and V_0 the sample volume.

4. Tensile test microcalorimetry

The microcalorimeter is placed directly on the cross-head of the testing machine in which the sample passes through the measurement cell. The main reason for such a device is that the measurements of the evolved heat are not performed between two thermal equilibrium states but continuously during the deformation of the specimen. The essential technical performance parameters are the cell sensitivity and the thermoregulation efficiency.

The cell consists of two coaxial copper cylinders, which are electrically insulated. Between the cylinders, 12 thermocouple bars are immersed into heat-insulated moss. Around 1200 thermocouples are distributed in a regular manner on both surfaces (Fig. 2).

To obtain the best signal-to-noise ratio, the thermoregulation was carried out carefully. The test room must be completely closed. The air was

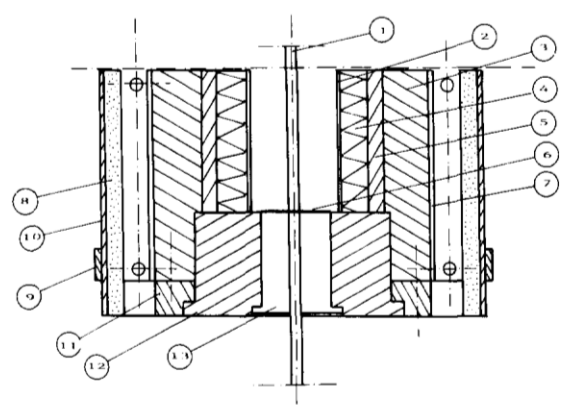

Fig. 2. Microcalorimeter cell: 1, sample; 2, internal cell cylinder; 3, aluminium block; 4, thermocouples; 5, external cell cylinder; 6, antiradiation screen; 7–13, thermal resistances.

circulated using six electric fans and the temperature controlled with two heat sources. The signal quality is improved by a series of thermal resistances placed between the test room air and the cell. The fluctuations in signal due to interactions with the surroundings correspond to temperature variations in the cell of around 10^{-3} °C. Its maximum amplitude was around several microvolts and cannot be recorded directly. Therefore a two-stage low level thermocouple amplifier was built. The first-stage gain is around 10^3 and uses an INA101 modulus enclosed in an isothermal copper box (electrostatic shield). The amplifier was connected to the cell with very short shielded wires, in order not to intercept parasitic inductions of the same order of magnitude as the signal which would then be amplified. The second stage is a more classical linear integrated circuit amplifier (Fig. 3).

5. Principle

To establish a relationship between the signal given by the thermopile and the heat evolved in the cell, several hypotheses are made. It is assumed that the heat transfers due to radiation, convection and conduction are well modelled by linear laws in temperature, in the vicinity of thermal equilibrium. Therefore, if T_i and T_e respectively are the mean temperatures of the internal and external cell cylinders, the signal s is proportional to the thermal disequilibrium:

$$s = G(T_i - T_e) \tag{8}$$

where G is a proportionality constant.

Integrating the heat conduction equation, firstly in the deformed volume of the sample, secondly in the internal cell cylinder and finally in the external cell cylinder yields the following differential system:

$$\begin{aligned} &\mu_1 \dot{T}_m + H_1(T_m - T_i) + H_2(T_m - T_a) = \dot{W}_{ch} \\ &\qquad\qquad = \dot{W}_d - \dot{W}_{is} \\ &\mu_2 \dot{T}_i + H_3(T_i - T_e) - H_1(T_m - T_i) = 0 \\ &\mu_3 \dot{T}_e + H_4(T_e - T_a) - H_3(T_i - T_e) = 0 \end{aligned} \tag{9}$$

where T_m is the mean temperature of the strained sample, and where the test room temperature is assumed to be constant; μ_1, μ_2 and μ_3 respectively are the heat capacities of the sample, of the internal cell cylinder and of the external cell cylinder; H_1, H_2, H_3 and H_4 characterize the linear heat transfers in the cell (Fig. 4). The variations in the heat transfer coefficients during the deformation process can be neglected as long as the strain does not exceed 10%.

Then, if eqns. (8) and (9) are taken into account, the relationship between W_{ch} and s can be deduced:

$$t_a \dot{s}(t) + s(t) + \int_0^t \left[\frac{1}{t_b} + \frac{1 - t_a/\tau_2}{\tau_1} \exp\left\{ \frac{-(t-x)}{\tau_2} \right\} \right] \times s(x)\, dx = K W_{ch}(t) \tag{10}$$

where

$$\tau_1 = \frac{\mu_3}{H_3}$$

$$\tau_2 = \frac{\mu_3}{H_4}$$

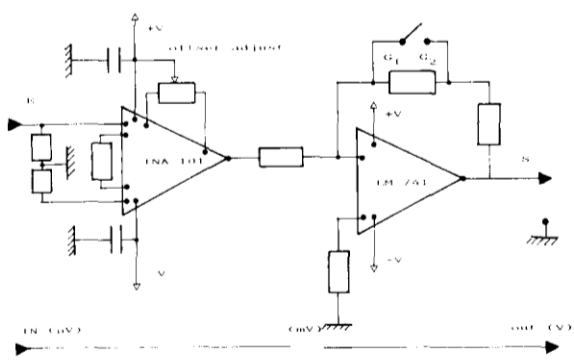

Fig. 3. Two-stage low level thermocouple amplifier.

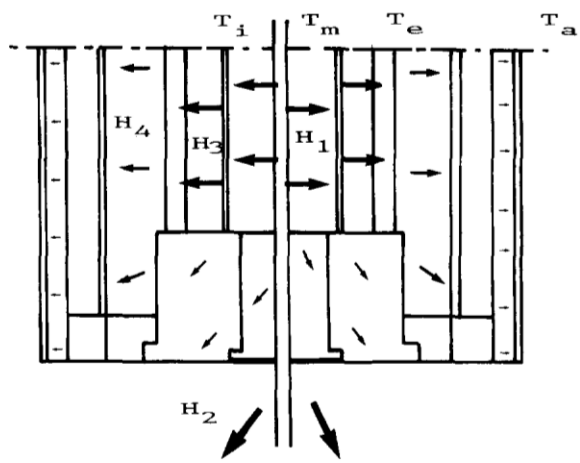

Fig. 4. Basic sketch of the linear heat transfers modelling in the calorimeter cell.

$$\delta^{-1} = \mu_1(H_1 + H_3) + \mu_2(H_1 + H_2)$$

$$t_a = \delta\mu_1\mu_2 \qquad (11)$$

$$\frac{1}{t_b} = (H_1H_2 + H_1H_3 + H_2H_3)\,\delta$$

$$K = \delta G$$

and where $H_3/H_1 \ll 1$. The constants τ_1 and τ_2 do not depend on the sample characteristics and are evaluated once and for all.

6. Calibration

As a calibration technique, we use the thermoelastic effects. For elastic loading, the heat source is so small that T_e is assumed to be constant. A simplified form of eqn. (10) is

$$t_a\dot{s}(t) + s(t) + \int_0^t \frac{s(x)}{t_b}\,dx = KW_{ch}(t) \qquad (12)$$

During monotonic loading or unloading, K and t_b can be experimentally evaluated; the heat source is known:

$$\dot{W}_{ch} = \dot{W}_0\{H(t) - H(t-\alpha)\} \qquad (13)$$

where H is the Heaviside function, and $\dot{W}_0 = -V_0\lambda\{\sigma(t) - \sigma(0)\}/(\alpha)T_a$, α being the loading duration.

The signal evolution can be analytically established:

$$s(t) = K\dot{W}_0\left[t_b + \frac{1}{\Delta^{1/2}}\left\{\frac{\exp(p_1t)}{p_1} - \frac{\exp(p_0t)}{p_0}\right\}\right] \quad \text{for } 0 \leqslant t \leqslant \alpha$$

$$s(t) = \frac{K\dot{W}_0}{\Delta^{1/2}}\left[\frac{\exp(p_1t)}{p_1\{1-\exp(-p_1\alpha)\}} - \frac{\exp(p_0t)}{p_0\{1-\exp(-p_0\alpha)\}}\right] \quad \text{for } \alpha \leqslant t \qquad (14)$$

where

$$\Delta = 1 - \frac{4t_a}{t_b}$$

$$p_0 = \frac{-1-\Delta^{1/2}}{2t_a} \leqslant 0$$

$$p_1 = \frac{-1+\Delta^{1/2}}{2t_a} \leqslant 0$$

An analysis of the experimental response $s(t)$ gives an order of magnitude for t_a and t_b so that $t_a \ll t_b$. If α is imposed in such a way that $\alpha \ll t_b$, the restitution of thermal equilibrium can agree perfectly with an exponential law:

$$s(t) \approx s(t_M)\exp\left(\frac{-(t-t_M)}{t_b}\right) \qquad (15)$$

where $s(t_M)$ represents the maximum deviation reached for s at t_M and is defined by

$$s(t_M) \approx K\dot{W}_0\left(1 - \frac{t_M}{t_b}\right) \qquad (16)$$

Exponential regression gives t_b, and experimental determination of $M(t_M, s(t_M))$ allows us to calculate the coefficient K (Table 1).

For elastic cyclic loading, a periodic square source can be obtained:

$$\dot{W}_{ch}(t) = \dot{W}_0\left\{H(t) + 2\sum_{k=1}^{\infty}(-1)^kH(t-k\alpha)\right\}. \qquad (17)$$

When t tends to infinity, the unstationary terms vanish and the signal tends to a period nature:

$$s(t) = K\dot{W}_0\left[t_b - 2\frac{\exp\{p_0(t-2k\alpha)\}}{\Delta^{1/2}\{1+\exp(\alpha p_0)\}} + 2\frac{\exp\{p_1(t-2k\alpha)\}}{\Delta^{1/2}\{1+\exp(\alpha p_1)\}}\right] \quad \text{for } 2k\alpha \leqslant t \leqslant (2k+1)\alpha \qquad (18)$$

TABLE 1 Determination of t_b and K for stainless steel A316L

Test	W_{is} (J)	K (deg K^{-1})	t_b (s)	*Correlation*
AI001	5.80	24.93	1481	0.98
AI002	7.12	18.26	2035	0.96
AI003	6.60	22.15	1858	0.98
AI004	6.37	22.00	2033	0.98
AI005	7.37	22.20	1703	0.98
AI006	6.97	20.00	1913	0.98
AI007	7.24	21.89	1701	0.98
AI008	7.32	22.10	1650	0.99

$$s(t) = K\dot{W}_0\left(-t_b + 2\frac{\exp[p_0\{t-(2k+1)\alpha\}]}{\Delta^{1/2}(1+\exp p_0)} - 2\frac{\exp[p_1\{t-(2k+1)\alpha\}]}{\Delta^{1/2}(1+\exp p_1)}\right)$$

$$\text{for } (2k+1)\alpha \leqslant t \leqslant 2(k+1)\alpha$$

The mechanical loading is reversed at each $t_n = n\alpha$; the signal extremum s_n will be reached as soon as $ds/dt(t = t_n^* \geqslant t_n) = 0$.

Equations (18) give

$$t_n(t_a, t_b) = t_n^* - t_n = \frac{t_a}{\Delta^{1/2}} \log\left\{\frac{1+\exp(\alpha p_1)}{1+\exp(\alpha p_0)}\right\} \quad (19)$$

If t_b is evaluated from eqn. (15), the measurement of t_n for different loading frequencies $(2\alpha)^{-1}$ allows t_a to be determined. Some results are shown in Table 2 and illustrated in Fig. 5.

7. Results

Tests on two industrial materials used industrially: age-hardened stainless steel A316L or age-hardened cabon steel XC38 were carried out. The evolved heat measurements were compared with the results obtained locally using an IR device [8]. The measurements are presented in Tables 3 and 4 for the two steels, and Figs. 6 and 7 illustrate the energy balance evolution. The relative accuracies of the anelastic and the isentropic energy measurements are relatively small (around 2%); the difference between the total amounts of heat measured by the two experimental approaches is naturally more important. The minimum and maximum values are indicated in the tables. The difference between the values is around 40 J for the largest strain for both steels; this represents a maximum relative accuracy of around 25% (for both steels). The stored energy evaluation is obtained as the difference between the anelastic work and the dissipated energy (see eqns. (4)–(7)). The extremal values are also indicated in the tables. In Fig. 8 the spread of the stored energy against the tensile stress is bounded by the two curves and is shown as a shaded area. In Figs. 9 and 10 the ratio $F = W_s/W_a$ of the stored energy to the anelastic energy is plotted as a function of the tensile strain. The shaded areas in these plots represent the absolute errors.

TABLE 2 Determination of t_a for stainless steel A316L

Test	2α (s)	ν (Hz)	Δt_{min} (s)	Δt_{max} (s)
CY001	47.5	2.1×10^{-2}	19.2	20.0
CY002	72.0	1.4×10^{-2}	22.8	25.8
CY003	95.0	1.1×10^{-2}	28.8	34.2
CY004	143.5	7.0×10^{-3}	33.0	39.0
CY005	237.0	4.2×10^{-3}	43.5	50.0
CY006	360.0	2.7×10^{-3}	48.0	55.0
CY007	474.0	2.1×10^{-3}	57.0	63.0
CY008	720.0	1.4×10^{-3}	57.0	69.0
CY009	952.0	1.0×10^{-3}	50.0	65.0
CY010	1200.0	8.4×10^{-4}	54.0	74.0
CY011	1432.0	7.0×10^{-4}	54.0	84.0

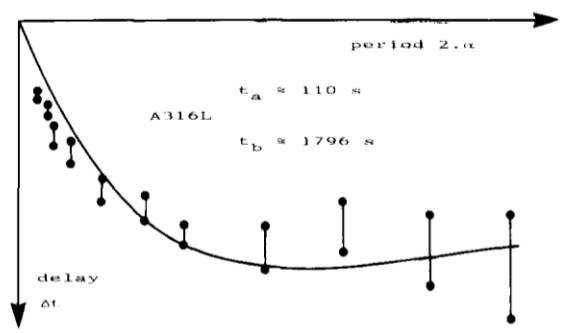

Fig. 5. Microcalorimeter calibration: determination of t_a for the age-hardened stainless steel.

TABLE 3 Energy balance evolution for stainless steel A316L

ε (%)	W_a (J)	$-W_{is}$ (J)	W_{ch} (J)		W_s (J)		F (%)		σ (MPa)
			Micro-calorimetry	IR	Micro-calorimetry	IR	Micro-calorimetry	IR	
1	16.3	−10.0	0.8	−2.2	5.5	8.5	30	52	290
3	64.3	−12.6	33.7	18.7	18	33	28	51	346
5	135.7	−14.4	86.3	61.3	35	60	26	44	390
7	205.4	−16.1	134	101	55	88	27	43	428
9	277.5	−17.7	183	147	77	113	27	41	466

TABLE 4 Energy balance evolution for carbon steel XC38

ε (%)	W_a (J)	$-W_{is}$ (J)	W_{ch} (J)		W_s (J)		F (%)		σ (MPa)
			Micro-calorimetry	IR	Micro-calorimetry	IR	Micro-calorimetry	IR	
1	25.5	−12.0	3.3	−1.8	10.2	15.3	40	60	410
2	62.0	−13.3	27.2	19.7	21.5	29.0	35	47	451
3	98.3	−14.3	59.0	41.0	25	43	26	44	482
5	182.4	−15.8	126.6	94.6	40	72	22	39	528
7	274.4	−16.9	198	160	60	98	22	36	560

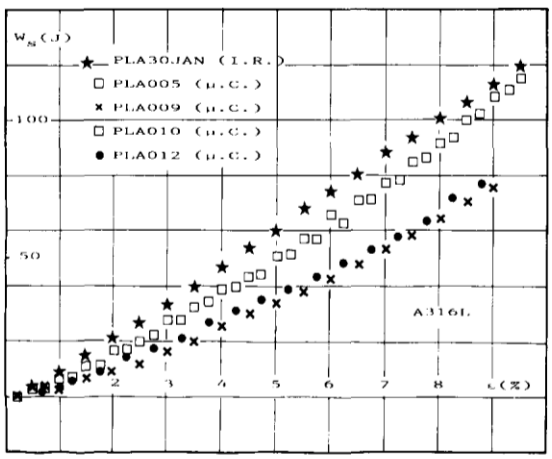

Fig. 6. Stored energy evolution for age-hardened stainless steel deduced from IR and microcalorimetry measurements (equivalent sample volume $V_0 = 8.4 \times 10^{-6}$ m^3).

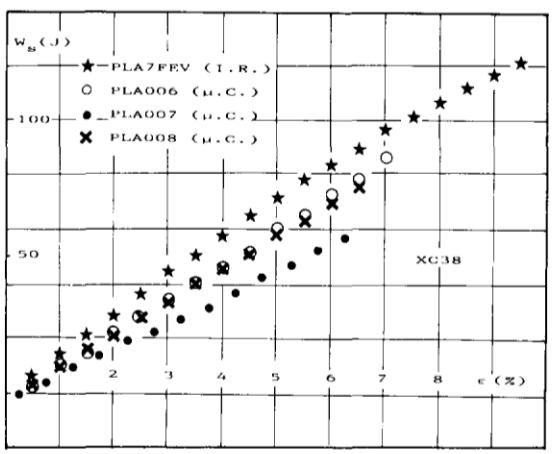

Fig. 7. Stored energy evolution for age-hardened carbon steel and deduced from IR and microcalorimetry measurements (equivalent sample volume $V_0 = 8.4 \times 10^{-6}$ m^3).

8. Discussion

The different criteria which have been taken into account to control the validity of constitutive equations of classical behaviour models or to

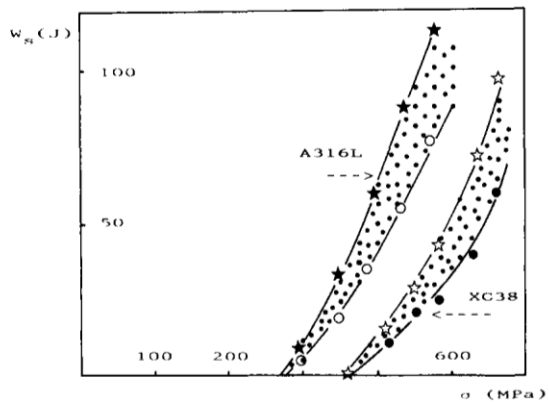

Fig. 8. The stored energy as a function of tensile stress for stainless steel (★, ○) and carbon steel (☆, ●).

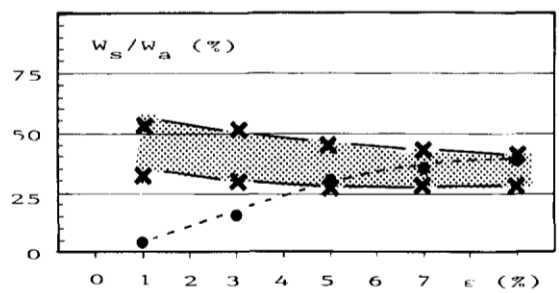

Fig. 9. Observed decrease in the stored energy ratio as a function of strain (spread, shaded area), and its increase predicted by classical models (– – –), for stainless steel.

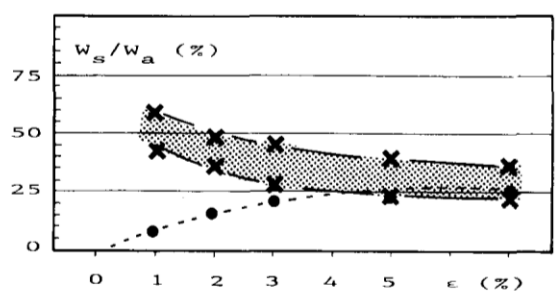

Fig. 10. Observed decrease in the stored energy ratio as a function of strain (spread, shaded area), and its increase predicted by classical models (– – –), for carbon steel.

proposed new constitutive thermomechanical models, are as follows.

(1) The amount of stored energy increases with increasing extent of tensile deformation in such a way that its ratio to the anelastic energy is a decreasing function of strain.

(2) The ratio F reaches around 50% at the beginning of strain hardening and represents during the transformation a large part of the mechanically expended energy ($20 \leqslant F \leqslant 60$):

$$\lim_{\varepsilon_p \to 0} \left(\rho \frac{\partial \psi}{\partial \alpha_j} \dot{\alpha}_j \right) \approx 0.5 \sigma : \dot{\varepsilon}_p \tag{20}$$

(3) Because of the spread in the measurements, a linear dependence of the stored energy on the tensile stress is adopted, as a first approximation.

If the decrease in the stored energy ratio is now a classical result [1], the percentages obtained here (on age hardening polycrystals etc.) are more important than those often cited by the metallurgists in the literature and obtained generally for annealed single crystals. In such a case, F does not exceed 15%; this explains the classical concept of considering the stored energy evolution to be negligible and not taking it into account during the determination of the constitutive equations of the behaviour law. Such a concept leads to

$$\dot{w}_s = \rho \frac{\partial \psi}{\partial \alpha_j} \dot{\alpha}_j \ll \sigma \dot{\varepsilon}_p \ (\approx 0) \tag{21}$$

where w_s is the stored energy per unit volume.

Let us now consider the models which form the basis of the elastic–plastic behaviour modelling: the Prandtl–Reuss law (isotropic hardening), and the Prager law (linear kinematic hardening). Using the classical results of the generalized standard material theory [6], the two models lead to the following dissipation form, when the von Mises criterion is chosen, for a monotonic tensile test:

$$D_1 = \sigma_e \dot{\varepsilon}_p \qquad \text{for } \sigma \geqslant \sigma_e \tag{22}$$

$$w_d = \sigma_e \varepsilon_p \qquad \text{for } \sigma \geqslant \sigma_e \tag{23}$$

where σ_e is the yield stress, $\dot{\varepsilon}_p$ is the axial component of the plastic strain rate and w_d is the dissipated energy per unit volume. Both eqn. (4) and eqn. (22) allow us to determine the evolution of the stored energy rate:

$$\dot{w}_s = (\sigma - \sigma_e) \dot{\varepsilon}_p \qquad \text{for } \sigma \geqslant \sigma_e \tag{24}$$

Firstly, eqn. (24) contradicts eqn. (21) as soon as σ becomes large compared with σ_e. Secondly, it implies an obvious increase in the stored energy ratio, which is not in accordance with the experimental observations (see refs. 4 and 8). In Figs. 9 and 10, the broken curves represent the evolution of F defined by

$$F = \frac{W_s}{W_a} = \int_0^t (\sigma - \sigma_e) \dot{\varepsilon}_p \, d\tau \Big/ \int_0^t \sigma \dot{\varepsilon}_p \, d\tau \tag{25}$$

In the framework of the generalized standard material theory, modifications of both models have been proposed in order to predict reasonably the energy balance evolution. A linear correspondence between stored energy and tensile stress is adopted (however, a non-linear dependence could possibly be used): such an element enables us to identify completely the Helmholtz free energy as soon as an additive decomposition into elastic and plastic parts is allowed, when the temperature influence on the plastic part is negligible. This will not be discussed in detail here, but the use of such a phenomenological hypothesis has already been developed in refs. 8–10.

In conclusion, we emphasize the fact that a study of the energy balance associated with deformation processes is helpful in determining the consistency of the thermomechanical behaviour laws. The microcalorimeter presented here allows us to make such a continuous energy balance during the transformation, for simple mechanical loading (tension or torsion). It can be calibrated using several thermoelastic effects, which limits its utilization to materials possessing an elastic domain. However, its great sensitivity allows us to observe thermal effects at a very low strain rate. It can be used to study the energy balance during creep tests and torsional loading.

References

1 G. I. Taylor and H. Quinney, The latent energy of cold work, *Proc. R. Soc. London, Ser. A, 143* (1933) 307–328.

2 R. O. Williams, The stored energy in a deformed copper; the effect of grain size and silver content, *Acta Metall., 9* (1961) 949–957.

3 D. Rönnpagel and Ch. Schwink, Measurement of stored energy of copper single crystals by means of a new deformation calorimetry method, *Acta Metall., 9* (1961)

949–957.
4 M. B. Bever, D. L. Holt and A. L. Titchener, The stored energy of cold work, *Prog. Mater. Sci., 17* (1973).
5 E. Krempl, Inelastic work and thermomechanical coupling in viscoplasticity, in A. Sawzuk and G. Bianchi (eds.), *Plasticity Today,* Elsevier Applied Science, Barking, Essex, 1985, pp. 247–257.
6 B. Halphen and Q. S. Nguyen, Sur les matériaux standards généralisés, *J. Méc. Appl., 14* (1) (1975) 39–63.
7 P. Germain, Q. S. Nguyen and P. Suquet, Continuum thermodynamics, *J. Appl. Mech., 50* (1983) 1010–1020.
8 A. Chrysochoos, Dissipation et blocage d'énergie lors d'un écrouissage en traction simple, *Thèse d'Etat,* Montpellier, 1987.
9 J. Lemaitre and J. L. Chaboche, *Mécanique des Matériaux Solides,* Dunod, Paris, 1985.
10 A. Chrysochoos, G. Martin, O. Maisonneuve, J. C. Chezeaux and H. Caumon, Dissipative and non dissipative phenomena during an elastoplastic deformation process, *Nucl. Eng. Des.,* in the press.